Biophysical Journal, Volume *119*

Supplemental Information

Dye Transport through Bilayers Agrees with Lipid Electropore Molecular Dynamics

Esin B. Sözer, Sourav Haldar, Paul S. Blank, Federica Castellani, P. Thomas Vernier, and Joshua Zimmerberg

Dye transport through bilayers agrees with lipid electropore molecular dynamics

Esin B. Sözer[1,*], Sourav Haldar[2,3,*], Paul S. Blank[2], Federica Castellani[1, 4], P. Thomas Vernier[1†] and Joshua Zimmerberg[2‡]

[1]Frank Reidy Research Center for Bioelectrics, Old Dominion University, Norfolk, VA 23508, USA

[2]Section on Integrative Biophysics, *Eunice Kennedy Shriver* National Institute of Child Health and Human Development, Bethesda, MD 20892, USA

[3]Current address: Department of Biochemistry and Bioinformatics, GITAM Institute of Science, GITAM (Deemed to be University), Visakhapatnam-530045, Andhra Pradesh, India

[4]Biomedical Engineering Institute, Frank Batten College of Engineering and Technology Old Dominion University, Norfolk, VA 23529, USA

*These authors equally contributed to this work.

[†]Corresponding author: pvernier@odu.edu (PTV)

[‡]Corresponding author: zimmerbj@mail.nih.gov (JZ)

Supplementary Material

Experimental Methods

Electric field exposure. We used 100 µm diameter tungsten wire electrodes similar to our prior exposure system described earlier (Sözer et al. 2017, 2018, 2019). The separation between the electrodes was approximately 80 µm.

The calculated electric field values for a 1 kV potential difference between the electrodes placed on top of a glass coverglass are shown in Figure S1. The electric field value right above the glass surface in the mid-region of the electrodes is 10 MV/m, which will proportionally scale with higher potential differences. In our case 4.5 kV pulse for 2 ns pulse corresponds to 45 MV/m, and 3.5 kV pulse for 6 ns pulse corresponds to 35 MV/m.

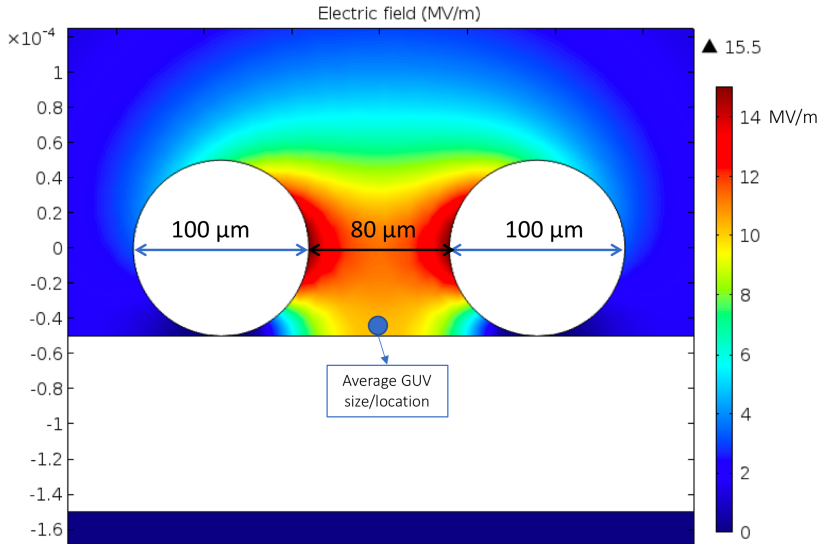

Figure S1 Electric field calculations between two tungsten wire electrodes with a potential difference of 1 kV.

GUV preparation. GUVs were prepared by the PVA-gel swelling method as described previously (Weinberger et al., 2013). Briefly, to prepare GUVs required, an amount of POPC drawn from a stock solution was diluted into 200 µl of $CHCl_3$ to a concentration of 3.94 mM (3.35 mg/ml). To this, 10 µl of DiD (Invitrogen) was added (from a stock of 5 µM in DMSO) and vortexed for ~2 min. This lipid mixture in $CHCl_3$ was then deposited on a plasma-cleaned (using a Harrick plasma cleaner, Ithaca, NY) microscope coverglass, coated with 5% (w/w in ddH_2O) polyvinylalcohol (Merck Millipore). The organic solvent was evaporated by a gentle stream of nitrogen and followed by storing in high vacuum for one hour. The coverglass with the lipid film on, was then transferred to a 30-mm tissue culture dish. 500 µl of PIPES buffer (1 mM EDTA, 1 mM HEDTA, 10 mM PIPES, 100 mM KCl, pH 7.4 with~200 mM sucrose) was added covering the entire surface of the coverglass and allowed to incubate for 30 minutes in the dark. After 30 minutes, the GUVs were harvested by gently tapping the sides of the dish, then gently drawing out using a 1 ml pipette without touching the surface and transferring them to a 1.5 ml micro-centrifuge tube. The GUV suspension was stored at 4°C until further use. The total lipid concentration of GUV suspension was 1.35 mg/ml (1.58 mM). Typically, GUVs were made the same day as the experiment.

For imaging, an aliquot of GUV suspension was added to an osmotically balanced glucose solution (1 mM EDTA, 1 mM HEDTA, 10 mM PIPES, 100 mM KCl, pH 7.4 with~200 mM glucose) to allow the GUVs to settle at the bottom of the imaging chamber.

Vesicle size correlation with fractional fluorescence change

Bioelectromagnetic theory predicts that a GUV (a spherical dielectric shell) in a uniform electric field in a conductive medium will develop a peak induced membrane potential proportional to its radius **(Pauly and Schwan 1959)**.

$$\Delta\psi_m = \frac{3}{2} E_0 r \,(1 - \, e^{-t/\tau_m}) \qquad \text{(S1)}$$

where ψ_m is the membrane potential, t is the duration of the electric field exposure, and τ_m is the membrane charging time constant. However, the positive correlation between vesicle radius and calcein fluorescence increase predicted by classical electroporation theory is not seen in our data

(Figure S2), in contrast to experiments where longer pulse durations were used **(Mauroy *et al.* 2012)**. This size-independence of membrane permeabilization is also seen in cells, when the pulse duration is much shorter than τ_m (approximately 100 ns in the current set of experiments). Mathematically, this comes from the linear approximation of the exponential term in equation S1 for small t/τ_m , since τ_m is directly proportional to vesicle size **(Sözer *et al.* 2017, Stewart *et al.* 2004)**. The negative correlation of vesicle size and fractional fluorescence change shown in Figure S2a is not significant when a smaller time range before and after pulse delivery is used to calculate fractional fluorescence change (Figure S2b and c). One interpretation is that a rapidly opening and closing pore population forms independent of vesicle size, causing an immediate fluorescence change at pulse delivery, and that the formation of longer-lasting (seconds) pores is negatively correlated with vesicle size. The reason for this dependence needs further investigation with a larger sample size. Note that we did not detect a change in vesicle size during our measurements. Nevertheless, the correlation calculations were done for the total transport after the very first pulse train delivery in Figure 2b, and the corresponding vesicle sizes were measured at the frame right before the pulse delivery, since we can only look for a correlation of the vesicle size with the transport at the instance of interaction with the external electric field.

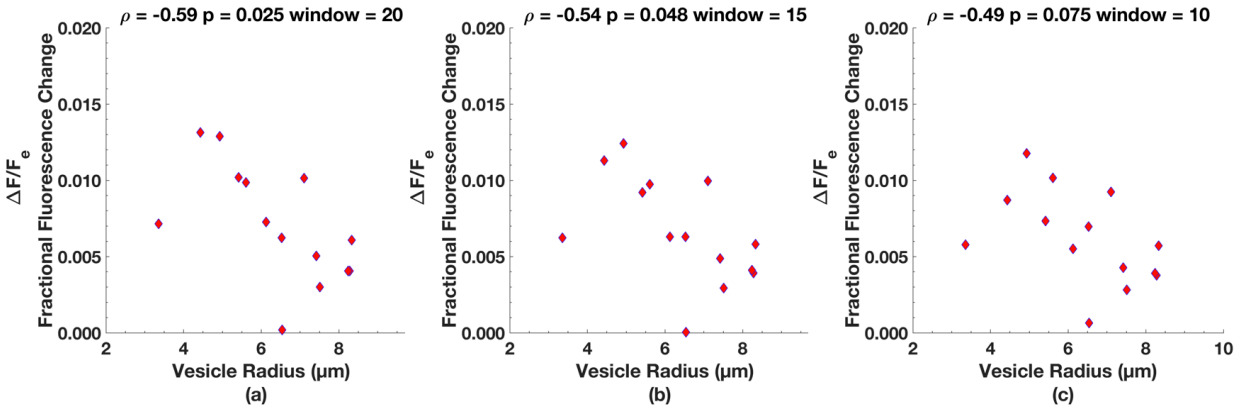

Figure S2 Vesicle size dependence of fractional fluorescence change calculated using window size (a)20 (b) 15 and (c) 10 around first pulse train delivery.

Kinetics of fluorescence change and electrodiffusion of calcein

From the kinetics presented in Figure 2b, we wonder if *6 ns (unipolar)* pulses form some longer lifetime pores (seconds) in the membrane in addition to a much larger number of fast-closing (tens of nanoseconds) pores. Longer lifetime pores can also explain the slower rise time of the responses to 2 ns bipolar pulses without any interpulse delay, which induces a high transmembrane potential across the membrane for 4-5 ns, resulting in the formation of a population of longer-lifetime pores similar to those produced by the unipolar 6 ns pulse exposures. Lipid pores with longer lifetimes are observed experimentally and in simulations when a low membrane potential is present **(Abidor *et al.* 1979, Sengel and Wallace 2016, Fernández *et al.* 2012).** This hypothesis suggests that longer duration pulses are more likely to form longer lifetime pores. See Figure S3 overlays of 6 ns unipolar and 2 ns bipolar waveforms and calcein uptake kinetics. A small population of longer lifetime pores with bipolar pulses without any interpulse delay is also consistent with MD simulations in which the electric field direction is reversed after pore formation. Field reversal did not affect pore size or lifetime. The pore continues to evolve as if the change in the direction of

the field did not happen. The longer lifetime pore population could also lead to a change in the system that affects response to subsequent pulse trains.

In contrast, with *2 ns unipolar* pulses in Figure 3 (either single or with 50 ns interpulse delay), the contribution of longer lifetime pores in the pore population is lower, thus we see sharp increases (faster than our recording speed of 1 fps) in calcein fluorescence intensity.

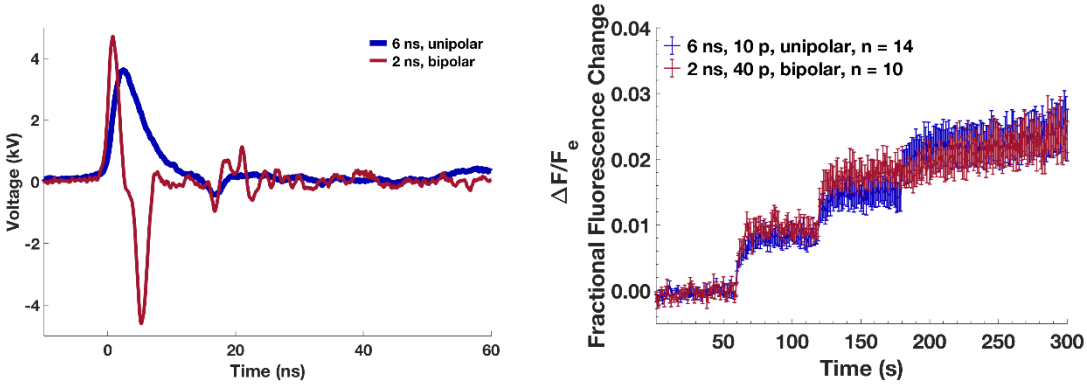

Figure S3. Left: overlay of 2 ns bipolar pulse with no interpulse delay and 6 ns unipolar pulse. Right: calcein uptake kinetics after exposure to two different pulse trains, consisting of the pulses shown on the left panel. Maroon: a train of 40 bipolar pulses (45 MV/m, 2 ns, 1 kHz repetition rate) were delivered at 60 and 120 seconds into the recording (also shown in the main manuscript figure 3). Blue: a train of ten unipolar pulses (35 MV/m, 6 ns, 1 kHz repetition rate) delivered at 60, 120 and 180 seconds into the recording (also shown in the main manuscript figure 2b).

The kinetic changes following pulse exposure to a train of ten pulses of 6 ns duration and field strength of 35 MV/m (Figure 2b) can be modeled as an "instantaneous" jump (unresolvable at 1 Hz imaging) at the start of a pulse sequence followed by a kinetic term with a single time constant. For the data presented in Figure 2b, both piecewise and global fitting support the hypothesis that the instantaneous jump, the contribution of the kinetic term, and the time constant are the same. The basic model is

$$IJ + A\,(1 - \exp\,(-t/\tau)) \qquad \text{(S2)}$$

where *IJ* is the "instantaneous" change measured in the first image frame, *A* is the amplitude associated with the kinetics resolved in subsequent image frames, and τ is the time constant. Table S1 summarizes the fitted data obtained using three parameter, piece-wise fitting, after subtracting the starting plateau value, and Figure S4 shows the data with the fit. Regression of all parameter values, as a function of pulse sequence also indicates no linear dependence (slope not statistically different from 0) supporting the hypothesis that each pulse sequence, on average, is an independent realization of the underlying creation of pores with approximately half of the signal change due to electrophoretic transport (drift) through short lived pores and the other half due to diffusive transport through longer lived pores.

Table S1 Three parameter piece-wise fitting of kinetics of fluorescence change after 6 ns, 35 MV/m pulse train (Fig 1b main manuscript) to equation S2

	Pulse Train		
ΔF/Fe	1	2	3
Amplitude (*A*)	0.005	0.003	0.004
Instantaneous Jump *(IJ)*	0.004	0.004	0.004
Total Change	0.009	0.007	0.007
95% Confidence	0.002	0.002	0.001
τ (s)	7.7	9.8	12.0
95% Confidence	3.5	7.3	5.2

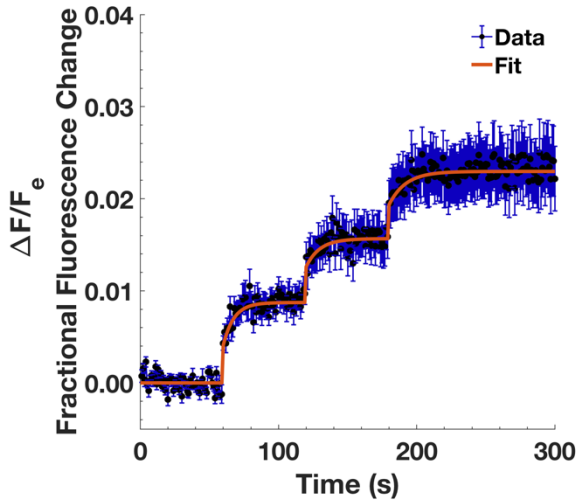

Figure S4. Three parameter piece-wise fitting of data from main manuscript Figure 2b where GUVs exposed to three 1 kHz trains of ten 6 ns electric pulses at field strengths of 35 MV/m, delivered 1, 2, and 3 minutes into the recording (n = 13).

We next consider whether the ~1% changes in fluorescence observed using 6 and 2 ns pulses are consistent with a population of transient pores of nanosecond duration undergoing electrodiffusion. Pore-mediated transport of calcein was modeled using a simple electro-diffusive transport model as described previously **(Sözer *et al.* 2018)**. Briefly, following the Nernst-Planck formalism $J_{p,}$ electrodiffusive transport through a single cylindrical pore was defined as sum of two components, the diffusion term ($J_{diffusion}$) and the drift term (J_{drift}):

$$J_p = J_{\text{diffusion}} + J_{\text{drift}} \tag{S3}$$

$$J_{\text{diffusion}} = \frac{\pi {r_{\text{pore}}}^2 D_s\, c}{l_{\text{pore}} + \frac{\pi r_{\text{pore}}}{2}} \tag{S4}$$

where D_s is the diffusion coefficient, r_{pore} is the pore radius, l_{pore} is the length of the pore (4 nm in these calculations), and c is the concentration difference from one side of the membrane to the other. The drift term is

$$J_{\text{drift}} = \frac{1}{2} \frac{\pi {r_{\text{pore}}}^2 D_s\, c}{l_{\text{pore}}} \frac{q_e z V_m}{kT} \tag{S5}$$

where V_m is the transmembrane potential, which can be estimated with equation S1 using the electric field amplitude and $r_{vesicle}$ vesicle radius, which is 6 μm on average in our experiments.

We assume that following electroporation, 2% of the vesicle's surface is populated by 1 nm pores ($n_{pore,fast}$ = 2.9e6) with a pore formation time of 0.5 ns, after which drift and diffusion processes begin. The drift lasts only as long as the duration of the pulse while diffusion continues for 50 ns. With these assumptions, we get the values in Table S2. If we assume a lower membrane potential with increasing pore numbers, we can derive, approximately, the same transport. For a continuum-based computational study on expected pore numbers for a variety of pulse durations, refer to Son et al. 2014.

Table S2 Calculations of electrodiffusion of calcein through short-lived pores

	6 ns, 35 MV/m, 10 p		2 ns, 45 MV/m, 40 p
V_m (V)	18	2	8
J_{drift} (mol/s)	2.2e-17	2.4e-18	9.7e-18
$J_{diffusion}$ (mol/s)	1.1e-20	1.1e-20	1.1e-20
$n_{pore,\ fast}$	2.9e6	2.9e7	2.9e6
$c_{intravesicular,drift,\ single\ pulse}$ (M)	3.8e-7	4.2e-7	4.6e-8
$c_{intravesicular,diffusion,\ single\ pulse}$ (M)	1.7e-9	1.8e-8	1.8e-9
$c_{intravesicular,\ pulse\ train}$ (M)	3.8e-6	4.4e-6	1.9e-6
$\Delta F/F_e$	0.02	0.02	0.01

These calculations show that the transport of calcein we observed as an instantaneous jump following the pulse sequence can be explained by transport through electropores with ~50 ns lifetime even when we limit the number of pores to a small fraction of the vesicle surface. The

slower kinetics (seconds) observed with 6 ns unipolar pulses are attributed to a much smaller number of longer lived pores undergoing diffusive transport alone.

For example, in the 6 ns pulse case if we replace half of the short-lived pores with only fifteen pores with a lifetime of 1 second at full transport capacity, we get approximately equal contribution of short and longer lifetime pores as listed in Table S3.

Table S3 Calculations of electrodiffusion of calcein through short-lived and longer-lived pores

	6 ns, 35 MV/m, 10 p
V_m (V)	18
J_{drift} (mol/s)	2.2e-17
$J_{diffusion}$ (mol/s)	1.1e-20
$n_{pore,\ fast}$	1.4e6
$n_{pore,\ slow}$	15
$c_{intravesicular,drift,\ single\ pulse}$ (M)	1.9e-7
$c_{intravesicular,diffusion,\ single\ pulse}$ (M)	1.9e-7
$c_{intravesicular,\ pulse\ train}$ (M)	3.8e-6
$\Delta F/F_e$	0.02

Molecular dynamics simulation time course of pore annihilation

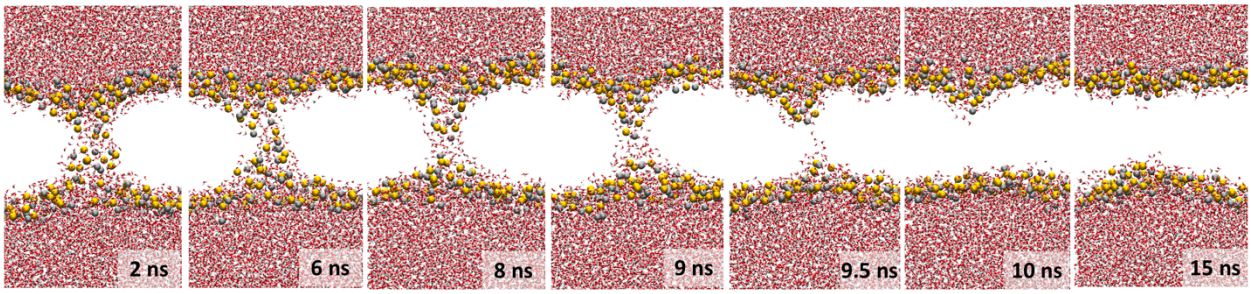

Figure S2 Snapshots of the evolution of a typical lipid electropore after removal of sustaining electric field. The pore shown is the same as the one in Figure 4b of the main manuscript (simulation plotted in red in Figure 4a, top plot). Pore collapse is complete at 10 ns for this pore. Red and white: water O and H; gold and silver: P and N of lipid head groups; lipid tails hidden for clarity.

References

Abidor IG, Arakelyan VB, Chernomordik LV, Chizmadzhev YA, Pastushenko VF, Tarasevich MR (1979) Electric breakdown of bilayer lipid membranes I. The main experimental facts and their qualitative discussion. Bioelectrochemistry Bioenerg 6:37–52.

Fernández ML, Risk M, Reigada R, Vernier PT (2012) Size-controlled nanopores in lipid membranes with stabilizing electric fields. Biochem Biophys Res Commun 423:325–330.

Mauroy C, Portet T, Winterhalder M, Bellard E, Blache M-C, Teissié J, Zumbusch A, Rols M-P (2012) Giant lipid vesicles under electric field pulses assessed by non invasive imaging. Bioelectrochemistry 87:253–259.

Pauly H, Schwan HP (1959) Über die Impedanz einer Suspension von kugelförmigen Teilchen mit einer Schale. Zeitschrift fur Naturforsch - Sect B J Chem Sci 14:125–131.

Sengel JT, Wallace MI (2016) Imaging the dynamics of individual electropores. Proc Natl Acad Sci 113:5281–5286.

Son, R.S., K.C. Smith, T.R. Gowrishankar, P.T. Vernier, and J.C. Weaver. 2014. Basic features of a cell electroporation model: illustrative behavior for two very different pulses. J. Membr. Biol. 247: 1209–1228.

Sözer EB, Levine ZA, Vernier PT (2017) Quantitative limits on small molecule transport via the electropermeome measuring and modeling single nanosecond perturbations. Sci Rep 7:57.

Sözer EB, Pocetti CF, Vernier PT (2018) Transport of charged small molecules after electropermeabilization - drift and diffusion. BMC Biophys 11:4.

Sözer EB, Vernier PT (2019) Modulation of biological responses to 2 ns electrical stimuli by field reversal. Biochim Biophys Acta - Biomembr 1861:1228–1239 .

Stewart DA, Gowrishankar IR, Weaver JC (2004) Transport lattice approach to describing cell electroporation: Use of a local asymptotic model. IEEE Trans Plasma Sci 32:1696–1708.

Weinberger A, Tsai F-C, Koenderink GH, Schmidt TF, Itri R, Meier W, Schmatko T, Schröder A, Marques C (2013) Gel-Assisted Formation of Giant Unilamellar Vesicles. Biophys J 105:154–164 .